



HAL
open science

Mapping the rheology of the Central Chile subduction zone with aftershocks

William B. Frank, Piero Poli, Hugo Perfettini

► **To cite this version:**

William B. Frank, Piero Poli, Hugo Perfettini. Mapping the rheology of the Central Chile subduction zone with aftershocks. *Geophysical Research Letters*, 2017, 44, pp.5374-5382. 10.1002/2016GL072288 . insu-03596069

HAL Id: insu-03596069

<https://insu.hal.science/insu-03596069>

Submitted on 3 Mar 2022

HAL is a multi-disciplinary open access archive for the deposit and dissemination of scientific research documents, whether they are published or not. The documents may come from teaching and research institutions in France or abroad, or from public or private research centers.

L'archive ouverte pluridisciplinaire **HAL**, est destinée au dépôt et à la diffusion de documents scientifiques de niveau recherche, publiés ou non, émanant des établissements d'enseignement et de recherche français ou étrangers, des laboratoires publics ou privés.

Copyright

RESEARCH LETTER

10.1002/2016GL072288

Key Points:

- Dense aftershock catalog reveals how plate interface responds to megathrust earthquake
- Evolution of fault rheology, frictional parameters, and tectonic stressing rate constrained in depth
- Aseismic afterslip along the plate boundary complements coseismic deformation and drives aftershock activity

Supporting Information:

- Supporting Information S1
- Table S1

Correspondence to:

W. B. Frank,
wfrank@mit.edu

Citation:

Frank, W. B., P. Poli, and H. Perfettini (2017), Mapping the rheology of the Central Chile subduction zone with aftershocks, *Geophys. Res. Lett.*, *44*, 5374–5382, doi:10.1002/2016GL072288.

Received 8 DEC 2016

Accepted 18 MAY 2017

Accepted article online 22 MAY 2017

Published online 3 JUN 2017

Mapping the rheology of the Central Chile subduction zone with aftershocks

William B. Frank¹ , Piero Poli¹ , and Hugo Perfettini² 

¹Department of Earth, Atmospheric, and Planetary Sciences, Massachusetts Institute of Technology, Cambridge, Massachusetts, USA, ²Institut des Sciences de la Terre, Université Grenoble Alpes, CNRS, IRD, Saint-Martin-d'Hères, France

Abstract The postseismic deformation following a large ($M_w > 7$) earthquake is expressed both seismically and aseismically. Recent studies have appealed to a model that suggests that the aseismic slip on the plate interface following the mainshock can be the driving factor in aftershock sequences, reproducing both the geodetic (afterslip) and seismic (aftershocks) observables of postseismic deformation. Exploiting this model, we demonstrate how a dense catalog of aftershocks following the 2015 M_w 8.3 Illapel earthquake in Central Chile can constrain the frictional and rheological properties of the creeping regions of the subduction interface. We first expand the aftershock catalog via a 19 month continuous matched-filter search and highlight the log-time expansion of seismicity following the mainshock, suggestive of afterslip as the main driver of aftershock activity. We then show how the time history of aftershocks can constrain the temporal evolution of afterslip. Finally, we use our dense aftershock catalog to estimate the rate and state rheological parameter $(a - b)\sigma$ as a function of depth and demonstrate that this low value is compatible either with a nearly velocity-neutral friction ($a \approx b$) in the regions of the megathrust that host afterslip, or an elevated pore fluid pressure (low effective normal stress σ) along the plate interface. Our results present the first snapshot of rheology in depth together with the evolution of the tectonic stressing rate along a plate boundary. The framework described here can be generalized to any tectonic context and provides a novel way to constrain the frictional properties and loading conditions of active faults.

Plain Language Summary The slow postseismic deformation, or afterslip, that lasts several years following a major earthquake can be as strong as the earthquake itself and is therefore a key component in understanding the seismic hazard along tectonic plate boundaries. Afterslip is typically studied with GPS that measures the deformation at the surface, but with a low spatial precision. It is therefore difficult, if not impossible, to tease out the finer details of how the plate interface responds to a large earthquake and to identify which parts of the plate interface could rupture next. Here we develop a new framework to study what happens after a major earthquake using the precise evolution in time and space of aftershocks. We leverage the high-resolution aftershock distribution to determine how the friction of the plate boundary varies in depth, which allows us to better understand which parts of the plate interface are susceptible to afterslip. Our methods described here can be generalized to any tectonic plate boundary and provide a novel way to constrain how active faults are influenced by major earthquakes.

1. Introduction

The rheology along tectonic plate boundaries, which is controlled by many factors including lithology and fluid pressure, determines the frictional response to stress perturbations, such as large earthquakes [Dieterich, 1994; Collettini et al., 2011]. This can be seen as the brittle unstable deformation associated with the megathrust transitions to a rate-strengthening regime, where transient and/or continuous aseismic creeping is the dominant mode of tectonic release [Marone and Scholz, 1988; Marone et al., 1991; Hyndman et al., 1997; Scholz, 1998; Wech and Creager, 2011; Frank et al., 2015]. Both the rupture history of large megathrust earthquakes and the subsequent postseismic deformation are therefore strongly controlled by the fault rheology of the plate interface [Perfettini and Avouac, 2004a; Hsu et al., 2006; Perfettini and Avouac, 2007]. Modeling efforts in such a regime, where aftershocks are driven by afterslip on a rate-strengthening fault, suggest that it is possible to tease out the rheology and frictional properties of the plate interface with seismicity catalogs [Perfettini and Avouac, 2004a; Perfettini et al., 2005; Ariyoshi et al., 2007; Kato, 2007].

We study here the afterslip of the M_w 8.3 Illapel earthquake that struck Central Chile on 15 September 2015 [Tilmann *et al.*, 2016; Ruiz *et al.*, 2016; Barnhart *et al.*, 2016]. This event ruptured a ~ 200 km locked region [Métois *et al.*, 2016; Ruiz *et al.*, 2016] in between two zones of low coupling associated with ridges and fracture zones. A recent study of repeating earthquakes in Central Chile [Poli *et al.*, 2017] recognized localized regions of hydrated fractures around the main rupture area. These regions hosted several swarms during the 20 years before the Illapel earthquake, and following the mainshock, also accommodated intense aftershock activity and early afterslip [Barnhart *et al.*, 2016]. These observations highlight the major role played by rheological heterogeneity of the slab in modulating the interseismic plate coupling and afterslip.

We develop here a new framework to quantitatively infer the frictional properties of fault zones using seismological information. We first generate a dense catalog of aftershocks that accompanies the afterslip [Tilmann *et al.*, 2016; Barnhart *et al.*, 2016] following the 2015 M_w 8.3 Illapel earthquake. We then constrain the rheology along the subduction interface by analyzing this catalog in the context of a frictional afterslip model along a rate-strengthening fault.

2. Creating a Dense Aftershock Catalog

We analyze the continuous seismic data from 1 January 2015 (9 months before the Illapel mainshock on 16 September 2016) to 27 June 2016 at 15 three-component broadband seismic stations, all operating at 40 Hz within several hundred kilometers of the mainshock's epicenter (see Figure 1). The dense event catalog of seismic repeaters that we present here is generated through a two-step process: (i) we first obtain and analyze the catalog of earthquakes maintained by the Chilean Centro Sismológico Nacional (CSN) to establish a preliminary catalog of events; (ii) we then use high-quality waveforms from the initial catalog as templates in a continuous matched-filter search for repeating seismicity.

All the seismicity cataloged by the CSN (which include locations and arrival times) during the studied time period are candidate template events. We note that the large majority of candidate template events (982 of 1028 total) occur after the Illapel earthquake and are considered aftershocks. To determine whether we use a candidate event as a template, we first evaluate its signal-to-noise (SNR) ratio across the 15-station network (see supporting information S1). Because the goal of this analysis is to determine which candidate events to use as templates in a network-based matched-filter search, a candidate event must be made up of high-quality waveforms on at least five stations. Imposing this threshold results in 809 (out of 1028 total) template events that form our initial event catalog. We do not check the template events for redundancy at this stage so that our final event catalog will include as many different earthquakes as possible.

Matched-filter searches have been used in a wide variety of contexts where seismicity is known to repeat [Shelly *et al.*, 2007; Peng and Zhao, 2009; Frank *et al.*, 2014]. The matched-filter search consists of correlating template waveforms with continuous data in a sliding window that preserves the seismic moveout [Gibbons and Ringdal, 2006]. The resulting correlation coefficients of each trace are then summed to provide a time series that represents the similarity of the continuous data to the matched-filter template. We only use the seismic stations that recorded high-quality waveforms ($\text{SNR} > 10$) for each given template event to maximize the amount of information and ignore the noisy traces in the template waveforms. Given our method of estimating the SNR and establishing the template event catalog, this means that while the number of stations used for each template varies, a minimum of five stations are used.

Searching sample by sample, each of the 809 template events are used as templates over the 19 months of continuous 40 Hz seismic data. We use a daily detection threshold that is 10 times the median absolute deviation of the correlation coefficient sum to detect events significantly similar to the template. The waveforms associated with high enough correlation coefficients are then considered detected repeater events. All detected events are considered to have the same hypocenter (determined by the CSN) as their template.

Given that we did not check for redundancy among the template events, we suppose that there will be events in the repeating seismicity catalog that will be detected by multiple templates. To avoid this problem, we consider that any detected event within 10 s of another detection to be redundant. We note that this 10 s window concerns only the detection time, directly related to the arrival time, and not the event duration. We then compare the summed network correlation coefficients of a given group of redundant events and keep the event with the highest network correlation coefficient; all other redundant events from the catalog are eliminated. The matched-filter search using the initial catalog of template events yielded 32,817 events over

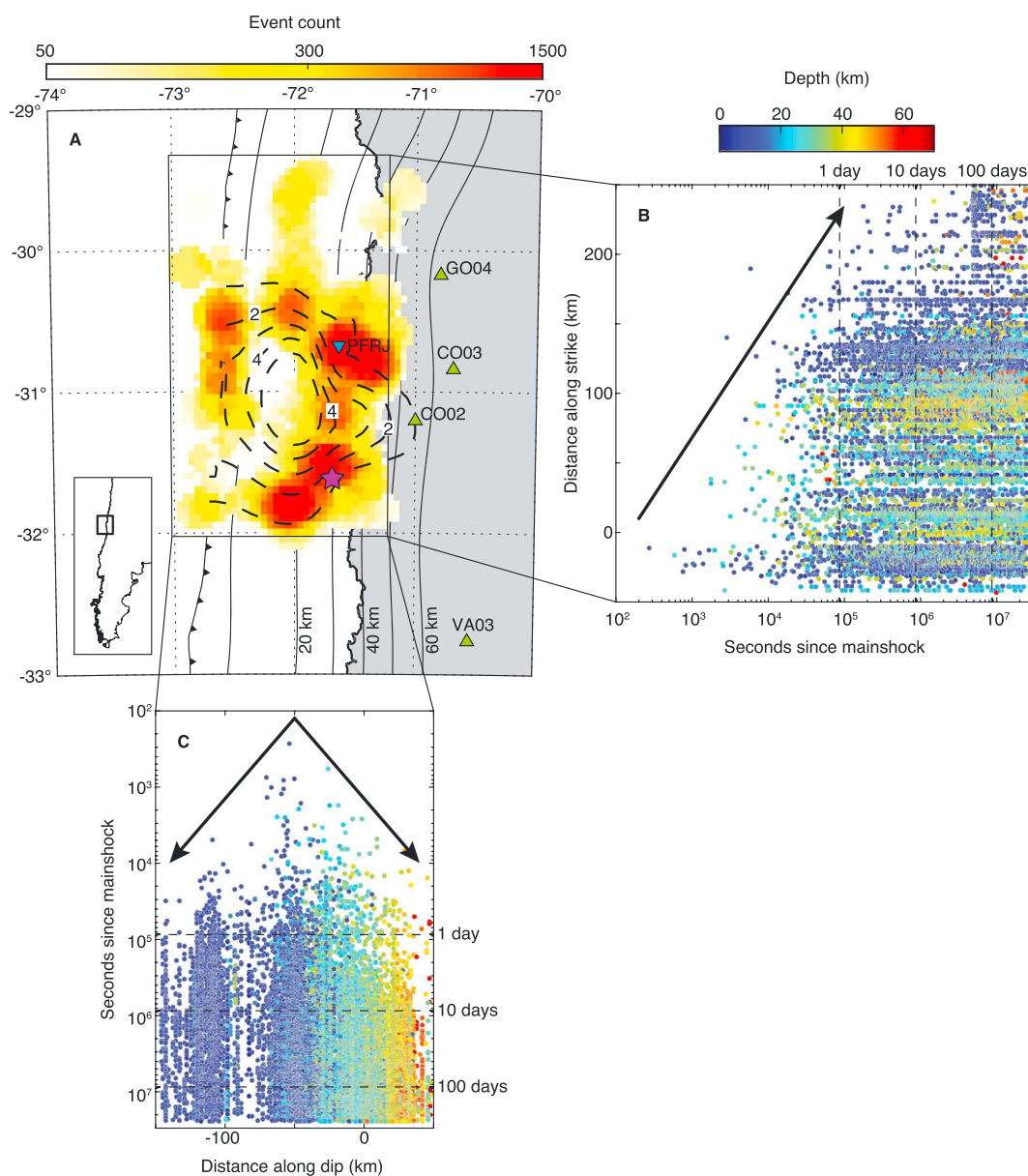


Figure 1. Distribution of coseismic slip and aftershocks for the 17 September 2015 M_w 8.3 Illapel earthquake in Central Chile. (a) The colors show the logarithmic distribution of aftershocks while the black dashed lines represent the coseismic slip distribution at 1 m intervals [Ruiz *et al.*, 2016]. The green triangles show 4 of the 15 seismic stations used. The blue inverted triangle indicates the GPS station PFRJ. The slab geometry is shown by the solid black contours [Hayes *et al.*, 2012]. The side panels show the semilogarithmic expansion of aftershocks, indicated as points colored by depth, (b) along strike and (c) along dip. The black arrows represent a semilogarithmic migration velocity away from the mainshock epicenter, shown as a purple star in Figure 1a.

the 19 month continuous seismic data set. After checking for event redundancy as described above, 16,132 events were included in our final catalog.

3. Temporal and Spatial Distribution of Aftershocks

Our final catalog of repeating seismicity contains 16,132 events (15,481 of which occur after the mainshock that we consider aftershocks), approximately 20 times more than the initial catalog of 809 events. Using the recently estimated afterslip moment of $4.2 \cdot 10^{20}$ N m [Shrivastava *et al.*, 2016] as a point of comparison, we find that the total moment associated with aftershocks over the same time period (43 days) is only $1.93 \cdot 10^{20}$ N m, or 46% of the aseismic moment. This suggests that the postseismic deformation is primarily aseismic and

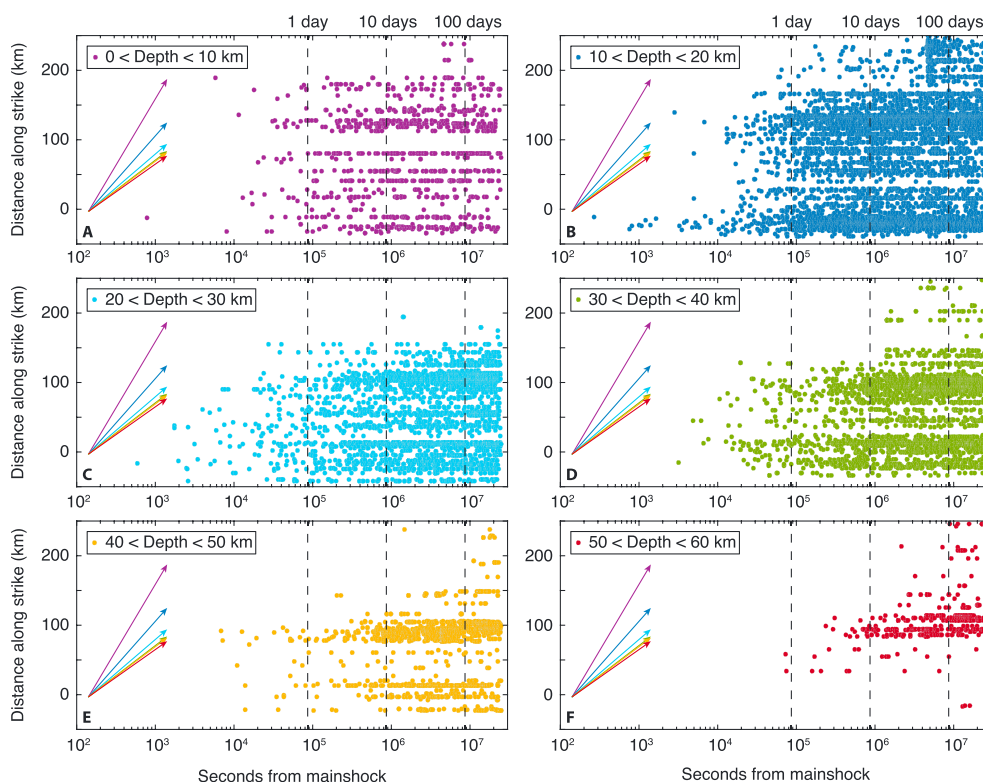


Figure 2. (a–f) Dependence of aftershock migration speeds with depth. Each panel shows the distribution of aftershocks along strike at different depths, indicated by the colors in the legends, as a logarithmic function of time since the mainshock. The colored arrows, corresponding to the different depth slices, show the migration speeds roughly estimated by eye.

controlled by the afterslip. We then remark that the seismicity almost perfectly outlines the main concentration of coseismic slip [Ruiz *et al.*, 2016] as shown in Figure 1. The spatial distribution of aftershocks also corresponds well with the distribution of afterslip [Tilmann *et al.*, 2016; Barnhart *et al.*, 2016; Shrivastava *et al.*, 2016] (see also Figure S1). The spatial distribution of the coseismic Coulomb stress changes does not correlate as well with the location of aftershocks, especially for the aftershocks south of the rupture area [Tilmann *et al.*, 2016] (see also Figure S2). We therefore suggest that the aftershocks illuminate the rate-strengthening regions of the fault, consistent with the idea that afterslip drives the production of aftershocks. These regions acted as barriers during the Illapel mainshock and preferentially rupture on a smaller spatial scale that matches the size of the brittle asperities that generate the aftershocks [Ruiz *et al.*, 2016; Barnhart *et al.*, 2016; Poli *et al.*, 2017].

We next highlight that the temporal evolution of the aftershocks, plotted in Figures 1b and 1c, shows a distinct log-time expansion both along strike and along dip. Numerical simulations have suggested that this semilogarithmic migration is indicative of afterslip-driven aftershock activity [Ariyoshi *et al.*, 2007; Kato, 2007] and subsequent observations have confirmed such [Peng and Zhao, 2009]. They also predict that the semilogarithmic migration speed is controlled by the rheology of the aseismically slipping fault.

To resolve whether there is a depth dependence of the aftershock migration, we plot the along-strike distance of the aftershocks as a function of time since the mainshock for six depth ranges in Figure 2. Estimating a rough migration velocity for each of the depth ranges, we observe that the aftershock migration speeds do indeed decrease with depth. This feature might be explained considering equation (29) of Perfettini and Ampuero [2008]. Considering the propagation of a stress perturbation of amplitude $\Delta\tau$ on a velocity-strengthening fault, this equation implies that the propagation velocity is proportional to $\exp(\Delta\tau/A')$, where $A' = (a - b)\sigma$ is the rheological parameter (see equation (2b)), a and b are the frictional parameters assuming a rate and state rheology, and σ is the effective normal stress. As σ is expected to increase with depth, this implies that the propagation velocity should decrease with depth as observed in Figure 2. We therefore suggest that the aftershock seismicity reveals an apparent slow down of afterslip expansion that reflects the changing

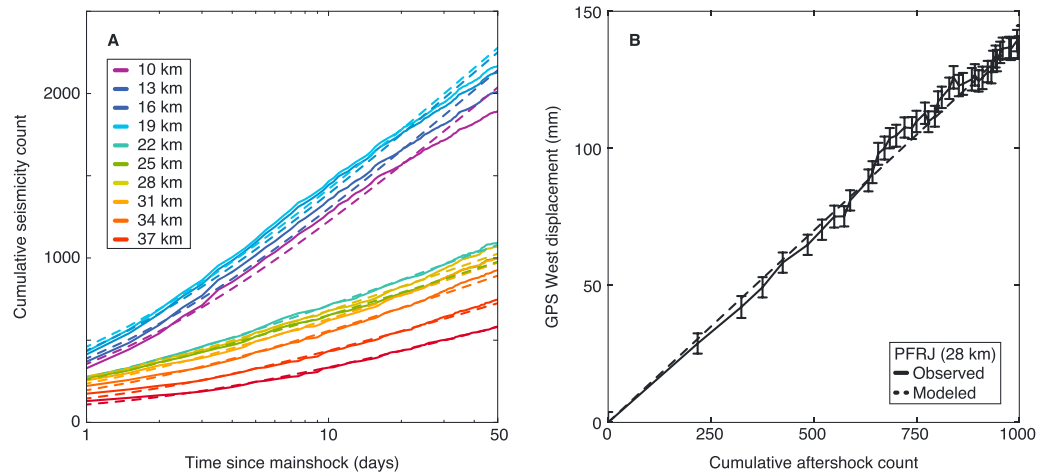


Figure 3. Afterslip evolution constrained by aftershock seismicity. (a) Seismicity evolution within different depth slices following the 2015 Illapel mainshock. The colored lines represent the observed (solid) and modeled (dashed) cumulative seismicity counts in different 20 km depth slices. The modeled seismicity counts are computed with the best fitting model parameters in equation (1), whose values are shown in Table S1 in the supporting information. (b) Validating the aftershock-determined parameters with the GPS-recorded afterslip evolution. Observed (solid with error bars) and modeled (dashed) GPS surface positions at PFRJ (see Figure 1) are plotted as a function of the closest depth-sliced aftershock catalog (28 km depth). The clear linear trends of the observed data that are predicted by the afterslip-driven aftershocks model and the good fits of the modeled data demonstrate the robustness of the aftershock-determined model parameters.

frictional properties along the subduction interface. To properly quantify these frictional parameters, we will now analyze the evolution of the aftershock seismicity.

4. Constraining Fault Rheology With Aftershocks

Assuming that seismicity is driven by the relaxation of the rate-strengthening regions of the fault, the cumulative number N_{cum} of aftershocks is given by *Perfettini and Avouac* [2004a]:

$$N_{cum}(t) = R_L t_r \log \left[1 + \frac{R_+}{R_L} \left(\exp \left(\frac{t}{t_r} \right) - 1 \right) \right], \quad (1)$$

where R_L is the long-term seismicity rate after the mainshock, R_+ is the seismicity rate right after the coseismic rupture, and t_r is the duration of the postseismic deformation. The parameters R_+ and t_r are given by:

$$t_r = \frac{A'}{\dot{\tau}}, \quad (2a)$$

$$A' = (a - b)\sigma, \quad (2b)$$

$$R_+ = R_L \exp \left(\frac{\Delta CFS}{A'} \right), \quad (2c)$$

where $\dot{\tau}$ and ΔCFS are, respectively, the stressing rate and Coulomb stress change (induced by the mainshock) on the rate-strengthening region.

To constrain A' , and therefore the rheology of the rate-strengthening regions along the subduction interface, we first divide our aftershock catalog into 10 subcatalogs that cover overlapping depth slices of 20 km. Assuming that the long-term seismicity rate is equal to the pre-mainshock rate R_L , we estimate R_L using the CSN seismicity catalog since January 2000 considering events with $M > 3$, the CSN catalog magnitude of completeness (see supporting information S1). We then perform a simple grid search of the two parameters R_+ and t_r of equation (1) to minimize an $L1$ misfit function between the observed and modeled cumulative aftershock counts. Given the logarithmic nature of equation (1), we use a logarithmically spaced time vector for the grid search. The best fit parameters reproduce well the cumulative seismicity counts as shown in Figure 3a. Table S1 gives the determined values of R_L , R_+ , and t_r , as well as the number of events N in each depth slice. The estimation of these parameters is robust as discussed in the supporting information.

This rate-strengthening model of afterslip predicts that the cumulative aftershock count is proportional to the surface displacement $U(t)$, whose evolution is [Perfettini and Avouac, 2004a]:

$$U(t) = U(t = 0) + \beta V_0 t_r \log \left[1 + \frac{R_+}{R_L} \left(\exp \left(\frac{t}{t_r} \right) - 1 \right) \right], \quad (3)$$

where β is a geometrical factor that scales the surface displacement and V_0 is the rate of tectonic convergence. We can therefore validate our aftershock-determined model parameters by computing the predicted surface displacement due to afterslip on the subduction interface, using β to scale $U(t)$ to the observed total displacement. Figures 3b and S3 show that the observed GPS displacements [Barnhart *et al.*, 2016] are remarkably well fit by the modeled displacements computed with equation (3). The model parameters that we determined via the aftershock seismicity are independently validated by the surface motion; we now consider their implications for the evolution of the subduction rheology in depth.

4.1. The Rheological Parameter A' in Depth

The average Coulomb stress increase ΔCFS for each depth slice is estimated considering the coseismic models of Shrivastava *et al.* [2016] and Ruiz *et al.* [2016], assuming that all aftershocks occur on faults with the same mean strike, dip, and rake as the mainshock (Figures S2, S4, and S9). This computation is further detailed in the supporting information. We remark the spatial anticorrelation between the coseismic slip models and the distribution of aftershocks/afterslip (see Figures S1 and S2). This spatial complementarity between independent data sets suggests that the rheological heterogeneities along the megathrust that control where seismic rupture occurs persist throughout the seismic cycle.

Equations (2a)–(2c) show that the stressing rate $\dot{\tau}$ and A' are related to the rest of the model parameters through:

$$A' = \frac{\Delta CFS}{\log \left(\frac{R_+}{R_L} \right)} \quad (4a)$$

$$\dot{\tau} = \frac{A'}{t_r} = \frac{1}{t_r} \times \frac{\Delta CFS}{\log \left(\frac{R_+}{R_L} \right)} \quad (4b)$$

and can be determined with our estimated values of ΔCFS , R_+ , R_L , and t_r for each depth slice. The distribution of $A' = (a - b)\sigma$ as a function of depth for both coseismic models is shown in Figure 4a. Both models' predictions are consistent and reflect the profile of the average coseismic Coulomb stress increase $\langle \Delta CFS \rangle$. This is not surprising as A' is not very sensitive to variations of R_+/R_L within the logarithmic denominator in equation (4a). Over a depth range of 40 km, the parameter A' varies weakly around 4×10^{-2} MPa. This value is slightly lower than previous estimates of A' (between 0.1 and 1 MPa) [Perfettini *et al.*, 2010, and references therein], but we suggest that our estimate is more reliable thanks to the much larger aftershock catalog analyzed here.

4.2. Tectonic Stressing Rate and Return Period of the Illapel Megathrust Segment

Figure 4b shows the distribution of the tectonic stressing rate within the creeping regions as a function of depth during the postseismic phase. The distribution of the stressing rates with depth for both coseismic models [Ruiz *et al.*, 2016; Shrivastava *et al.*, 2016] is consistent with a tectonic stressing rate that increases with depth. The stressing rate is initially nearly constant until 20 km depth with an average value of 4 kPa/yr. Beneath depths of 20 km, which corresponds roughly with the peak of the coseismic rupture, the stressing rate increases to a value of about 13 kPa/yr and then stagnates.

We determine a recurrence time T_{rec} for the Illapel megathrust segment using the coseismic stress drop along with the postseismic tectonic stressing rates discussed in the previous paragraph. Considering the mean stress drops $\Delta\tau$ predicted by the two coseismic models in the region where coseismic slip is greater 50% of the maximum, 0.3 MPa [Shrivastava *et al.*, 2016] and 0.24 MPa [Ruiz *et al.*, 2016], and the mean stressing rates $\langle \dot{\tau} \rangle$ of 9.23 kPa/yr and 7.6 kPa/yr from Figure 4b, we compute recurrence times T_{rec} of 32.5 and 31.5 years. The consistency of the inferred values for T_{rec} between the two models suggests that our estimation of T_{rec} is reliable. We also estimate T_{rec} via the interseismic coupling model of Métois *et al.* [2016] (see supporting information) and find a recurrence time of 56 years for the model of Shrivastava *et al.* [2016] and 43 years for the Ruiz *et al.* [2016] model.

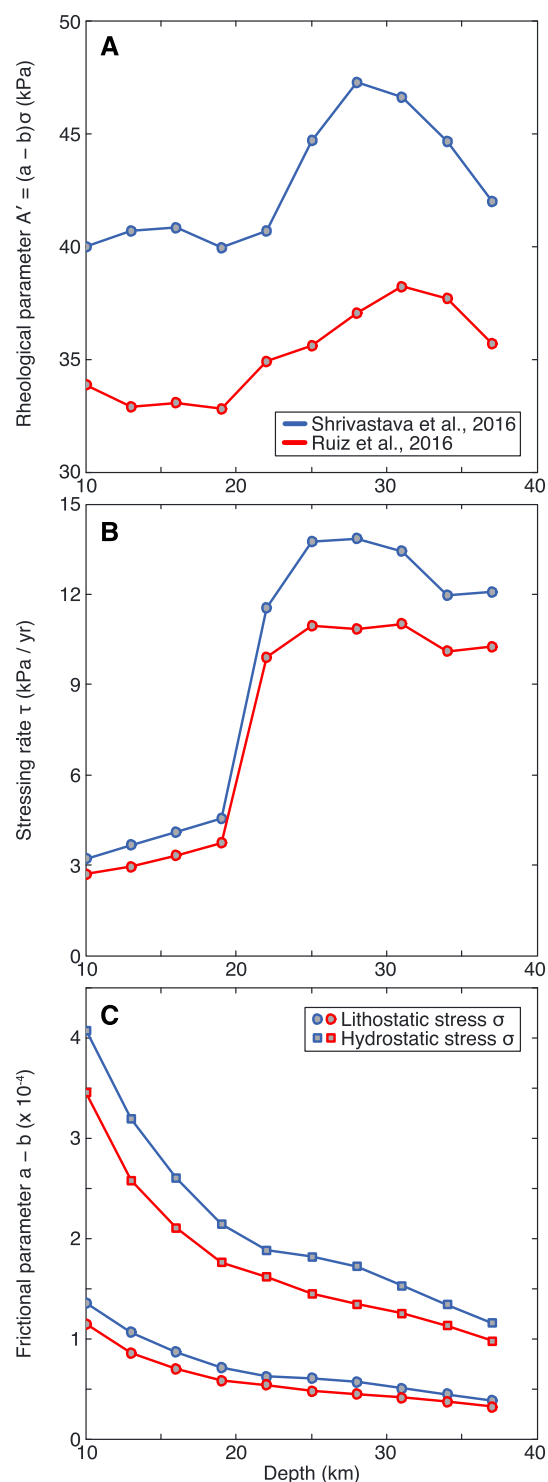


Figure 4. Evolution of rheology, tectonic loading, and friction along the Central Chile subduction. (a) Rheological parameter $(a - b)\sigma$ with depth determined with the cumulative aftershock counts in Figure 3, assuming the average Coulomb stress changes shown in Figure S4 that are estimated from the coseismic slip models of Shrivastava et al. [2016] (blue) and Ruiz et al. [2016] (red). (b) Tectonic stressing rate $\dot{\tau}$ with depth for each of the coseismic models. (c) Frictional parameter $(a - b)$ with depth for each of the coseismic models, assuming either lithostatic (circles) or hydrostatic (squares) stress σ .

Knowing that the last major earthquakes in this area struck in 1880 and 1943 [Ruiz et al., 2016], the recurrence time based on historical seismicity is about 60–70 years. Our estimate of T_{rec} based on the early postseismic deformation is about 32 years, half that of the historical recurrence time. This is not surprising as the stressing rate in the postseismic period is expected to be much larger than before the mainshock, corroborating the idea that the loading velocities along the plate interface are not constant [Frank, 2016] and potentially decay during the seismic cycle [Perfettini and Avouac, 2004b; Hetland and Simons, 2010]. The fact that the recurrence time T_{rec} derived from the late interseismic phase of the earthquake cycle is in rough agreement with the historical estimate suggests that the period of faster loading rates observed in the early postseismic phase is not representative of the mean loading regime of the Illapel segment. This idea is consistent with the Pisco (2007, M_w 8.0) and Maule (2010, M_w 8.8) earthquakes, where a quick return to preseismic velocities has been observed and interpreted as a rapid relocking of the rupture area [Remy et al., 2016; Bedford et al., 2016]. However, this might not be true for giant earthquakes such as the Valdivia (1960, M_w 9.5) and Anchorage (1964, M_w 9.1) earthquakes for which reports of large postseismic deformations are still observed nearly 40 years after the mainshock [Freymueller et al., 2000; Khazaradze et al., 2002], presumably due to deep viscoelastic relaxation [Perfettini and Avouac, 2004b].

4.3. Evolution in Depth of the Frictional Parameter $a - b$

The distribution of the frictional parameter $a - b$ for both coseismic models taking into account the effective normal stress σ is shown in Figure 4c. We assume that $\sigma = \rho gz$, where ρ is the volumetric mass, $g = 9.81 \text{ m/s}^{-2}$ the Earth gravity constant, and z is depth. Two end-member values of σ are computed with $\rho = 3000 \text{ kg/m}^3$ and $\rho = 1000 \text{ kg/m}^3$, corresponding respectively to lithostatic and hydrostatic

stresses. The evolution of $a - b$ is consistent for both models and shows a decrease of $a - b$ with depth. We note that the obtained distribution of the $a - b$ parameter as a function of depth (Figure 4c) represents an effective value of $a - b$ and that its true value must be much more heterogeneous given the collocation of seismic aftershocks and aseismic afterslip. While our derived values of $a - b$ are 1 to 2 orders of magnitude lower than laboratory estimates of $a - b$ (typically between 10^{-3} and 10^{-2}) [Marone, 1998], we believe that the estimates shown in Figure 4c are sound. The low values we find suggest that the active rate-strengthening regions are nearly velocity neutral ($a \approx b$). This feature is consistent with equation (2c) that shows that the increase in the seismicity rate R_+ induced by the mainshock is much larger (with an exponential dependence) in regions of lower $a - b$. An alternative explanation of the low value of $(a - b)\sigma$ is an elevated pore fluid pressure p that reduces the effective normal stress $\sigma = \sigma_{\text{litho/hydro}} - p$ [e.g., Poli et al., 2017]. We note that the $a - b$ parameter shows moderate variation with depth, justifying the assumption of a homogeneous value of this parameter at all depths [Perfettini and Avouac, 2007].

5. Conclusions

Studies of postseismic deformation typically rely on geodetic observations to constrain the distribution of afterslip but only capture the gross features of postseismic slip due to low spatial resolution. The dense aftershock catalog of the M_w 8.3 2015 Illapel earthquake we present here provides a unprecedented snapshot of the rheological properties along the Central Chile subduction zone as they change with depth. We show that the spatial distribution of aftershocks outlines the coseismic rupture patch, consistent with the idea that creeping, rate-strengthening regions arrest seismic slip. This feature, together with the observed logarithmic expansion of seismicity, demonstrates that the afterslip following the mainshock rupture is the main driver of aftershocks.

We show for the first time the variation of the frictional parameters with depth in a subduction zone, together with the stressing rate distribution that controls the motion on the plate interface. The mean stressing rates we find here that predict a faster recurrence than historical records is further proof that the loading rates during the megathrust earthquake cycle are not constant and change throughout the interseismic and post-seismic phases. The creeping regions that we characterize here are fundamental in assessing seismic hazard as they can arrest seismic rupture and control the production of aftershocks during postseismic deformation. Our results therefore constrain future numerical models of the seismic cycle. The methodology presented here forms a new framework that can easily be extrapolated to other regions of study where high-quality continuous seismic data sets are available.

Acknowledgments

We thank the Chilean Centro Sismológico Nacional for making their seismicity catalog available. We thank Mahesh Shrivastava and Emilie Klein for providing geodetic slip models and William Barnhart for providing GPS data. The continuous seismic waveforms used in this study were obtained through IRIS Data Services, which are funded through the Seismological Facilities for the Advancement of Geoscience and EarthScope (SAGE) Proposal of the National Science Foundation (NSF) under cooperative agreement EAR 1261681. The aftershock catalog produced here is available as a text file in the supporting information. The matched-filter processing was performed with the computational resources of the Massachusetts Green High Performance Computing Center. W.B.F. was supported by NSF grant EAR-PF 1452375. P.P. was supported by NSF grant EAR 1521534.

References

- Ariyoshi, K., T. Matsuzawa, and A. Hasegawa (2007), The key frictional parameters controlling spatial variations in the speed of postseismic-slip propagation on a subduction plate boundary, *Earth Planet. Sci. Lett.*, *256*(1), 136–146.
- Barnhart, W. D., J. R. Murray, R. W. Briggs, F. Gomez, C. P. Miles, J. Svarc, S. Riquelme, and B. J. Stressler (2016), Coseismic slip and early afterslip of the 2015 Illapel, Chile, earthquake: Implications for frictional heterogeneity and coastal uplift, *J. Geophys. Res. Solid Earth*, *121*, 6172–6191.
- Bedford, J., M. Moreno, S. Li, O. Oncken, J. C. Baez, M. Bevis, O. Heidbach, and D. Lange (2016), Separating rapid relocking, afterslip, and viscoelastic relaxation: An application of the postseismic straightening method to the Maule 2010 cGPS, *J. Geophys. Res. Solid Earth*, *121*, 7618–7638, doi:10.1002/2016JB013093.
- Colletini, C., A. Niemeijer, C. Viti, S. A. Smith, and C. Marone (2011), Fault structure, frictional properties and mixed-mode fault slip behavior, *Earth Planet. Sci. Lett.*, *311*(3), 316–327.
- Dieterich, J. (1994), A constitutive law for rate of earthquake production and its application to earthquake clustering, *J. Geophys. Res.*, *99*(B2), 2601–2618.
- Frank, W., N. Shapiro, A. Husker, V. Kostoglodov, H. Bhat, and M. Campillo (2015), Along-fault pore-pressure evolution during a slow-slip event in Guerrero, Mexico, *Earth Planet. Sci. Lett.*, *413*, 135–143.
- Frank, W. B. (2016), Slow slip hidden in the noise: The intermittence of tectonic release, *Geophys. Res. Lett.*, *43*, 10,125–10,133, doi:10.1002/2016GL069537.
- Frank, W. B., N. M. Shapiro, A. L. Husker, V. Kostoglodov, A. Romanenko, and M. Campillo (2014), Using systematically characterized low-frequency earthquakes as a fault probe in Guerrero, Mexico, *J. Geophys. Res. Solid Earth*, *119*, 7686–7700, doi:10.1002/2014JB011457.
- Freymueller, J. T., S. C. Cohen, and H. J. Fletcher (2000), Spatial variations in present-day deformation, Kenai Peninsula, Alaska, and their implications, *J. Geophys. Res.*, *105*(B4), 8079–8101.
- Gibbons, S. J., and F. Ringdal (2006), The detection of low magnitude seismic events using array-based waveform correlation, *Geophys. J. Int.*, *165*, 149–166, doi:10.1111/j.1365-246X.2006.02865.x.
- Hayes, G. P., D. J. Wald, and R. L. Johnson (2012), Slab1.0: A three-dimensional model of global subduction zone geometries, *J. Geophys. Res.*, *117*, B01302, doi:10.1029/2011JB008524.
- Hetland, E., and M. Simons (2010), Post-seismic and interseismic fault creep II: Transient creep and interseismic stress shadows on megathrusts, *Geophys. J. Int.*, *181*(1), 99–112.
- Hsu, Y.-J., M. Simons, J.-P. Avouac, J. Galetzka, K. Sieh, M. Chlieh, D. Natawidjaja, L. Prawirodirdjo, and Y. Bock (2006), Frictional afterslip following the 2005 Nias-Simeulue earthquake, Sumatra, *Science*, *312*(5782), 1921–1926.

- Hyndman, R., M. Yamano, and D. A. Oleskevich (1997), The seismogenic zone of subduction thrust faults, *Island Arc*, 6(3), 244–260.
- Kato, N. (2007), Expansion of aftershock areas caused by propagating post-seismic sliding, *Geophys. J. Int.*, 168(2), 797–808.
- Khazaradze, G., K. Wang, J. Klotz, Y. Hu, and J. He (2002), Prolonged post-seismic deformation of the 1960 great Chile earthquake and implications for mantle rheology, *Geophys. Res. Lett.*, 29(22), 2050, doi:10.1029/2002GL015986.
- Marone, C. (1998), Laboratory-derived friction laws and their application to seismic faulting, *Annu. Rev. Earth Planet. Sci.*, 26(1), 643–696.
- Marone, C., and C. H. Scholz (1988), The depth of seismic faulting and the upper transition from stable to unstable slip regimes, *Geophys. Res. Lett.*, 15(6), 621–624.
- Marone, C. J., C. H. Scholz, and R. Bilham (1991), On the mechanics of earthquake afterslip, *J. Geophys. Res.*, 96(B5), 8441–8452.
- Métois, M., C. Vigny, and A. Socquet (2016), Interseismic coupling, megathrust earthquakes and seismic swarms along the Chilean subduction zone (38°–18° S), *Pure Appl. Geophys.*, 173(5), 1431–1449.
- Peng, Z., and P. Zhao (2009), Migration of early aftershocks following the 2004 Parkfield earthquake, *Nat. Geo.*, 2(12), 877–881.
- Perfettini, H., and J.-P. Ampuero (2008), Dynamics of a velocity strengthening fault region: Implications for slow earthquakes and postseismic slip, *J. Geophys. Res.*, 113, B09411, doi:10.1029/2007JB005398.
- Perfettini, H., and J.-P. Avouac (2004a), Postseismic relaxation driven by brittle creep: A possible mechanism to reconcile geodetic measurements and the decay rate of aftershocks, application to the Chi-Chi earthquake, Taiwan, *J. Geophys. Res.*, 109, B02304, doi:10.1029/2003JB002488.
- Perfettini, H., and J.-P. Avouac (2004b), Stress transfer and strain rate variations during the seismic cycle, *J. Geophys. Res.*, 109, B06402, doi:10.1029/2003JB002917.
- Perfettini, H., and J.-P. Avouac (2007), Modeling afterslip and aftershocks following the 1992 Landers earthquake, *J. Geophys. Res.*, 112, B07409, doi:10.1029/2006JB004399.
- Perfettini, H., J.-P. Avouac, and J.-C. Ruegg (2005), Geodetic displacements and aftershocks following the 2001 $M_w = 8.4$ Peru earthquake: Implications for the mechanics of the earthquake cycle along subduction zones, *J. Geophys. Res.*, 110, B09404, doi:10.1029/2004JB003522.
- Perfettini, H., et al. (2010), Seismic and aseismic slip on the Central Peru megathrust, *Nature*, 465(7294), 78–81.
- Poli, P., A. M. Jeria, and S. Ruiz (2017), The M_w 8.3 Illapel earthquake (Chile): Preseismic and postseismic activity associated with hydrated slab structures, *Geology*, 45(3), 247–250.
- Remy, D., H. Perfettini, N. Cotte, J.-P. Avouac, M. Chlieh, F. Bondoux, A. Sladen, H. Tavera, and A. Socquet (2016), Postseismic relocking of the subduction megathrust following the 2007 Pisco, Peru, earthquake, *J. Geophys. Res. Solid Earth*, 121, 3978–3995, doi:10.1002/2015JB012417.
- Ruiz, S., et al. (2016), The seismic sequence of the 16 September 2015 M_w 8.3 Illapel, Chile, Earthquake, *Seismol. Res. Lett.*, 87(4), 1.
- Scholz, C. H. (1998), Earthquakes and friction laws, *Nature*, 391(6662), 37–42.
- Shelly, D. R., G. C. Beroza, and S. Ide (2007), Non-volcanic tremor and low-frequency earthquake swarms, *Nature*, 446(7133), 305–307.
- Shrivastava, M. N., et al. (2016), Coseismic slip and afterslip of the 2015 M_w 8.3 Illapel (Chile) earthquake determined from continuous GPS data, *Geophys. Res. Lett.*, 43, 10,710–10,719, doi:10.1002/2016GL070684.
- Tilmann, F., et al. (2016), The 2015 Illapel earthquake, Central Chile: A type case for a characteristic earthquake?, *Geophys. Res. Lett.*, 43, 574–583, doi:10.1002/2015GL066963.
- Wech, A. G., and K. C. Creager (2011), A continuum of stress, strength and slip in the Cascadia subduction zone, *Nat. Geo.*, 4(9), 624–628.